

1 **An artificial neural network model in predicting VTEC over Central Anatolia in**
2 **Turkey**

3 **Abstract**

4 In this research, the capability of the artificial neural networks to predict GPS VTEC
5 has been investigated over Central Anatolia in Turkey. The VTEC dataset was
6 derived from the 19 permanent GPS stations belonging to TUSAGA-Aktif and IGS
7 networks in the region. The study region extends in the area from west to east
8 bounded by longitudes of 36.2°E-37.5°E and from south to north bounded by latitudes
9 of 36.0°N-42.0°N. Considering the factors inducing VTEC variations in the
10 ionosphere, an artificial neural network was herein proposed that has seven input
11 neurons in a multi-layer perceptron model. The KURU and ANMU permanent GPS
12 stations from TUSAGA-Aktif network were selected to implement the neural network
13 model proposed. Based on the RMSE results achieved in the simulation tests with 50
14 attempts, the hidden layer in the NN model was designed to have 37 neurons since the
15 lowest RMSE was reached in this attempt. According to the correlation coefficients,
16 absolute and relative errors in the proposed neural network model, the NN VTEC are
17 quite well predicted in hourly and seasonal basis referring to the GPS VTEC. In
18 addition, this paper demonstrated that the NN VTEC model provides better
19 performance than the global IRI model presents. The selected GPS stations, ANMU
20 and KURU, in our GPS network demonstrate well-fitting with the proposed NN to
21 assist the improvement of regional models.

22 **Keywords:** GPS, Total Electron Content, GPS VTEC, Artificial Neural Network

23 **1. Introduction**

24 The ionospheric variations occurring within upper Earth's atmosphere is a
25 complicated phenomena caused by solar activity such as flares and CMEs (Coronal
26 Mass Ejections). Since the ionosphere has a dispersive feature, electromagnetic
27 transmissions such as GPS (Global Positioning System) signals propagating through
28 the ionosphere are exposed to delay. This delay is directly proportional to the TEC
29 (Total Electron Content) of the ionosphere along the path of the signal. It is described
30 that TEC is the total number of free electrons in a one-meter squared column

31 projected along the signal path between the source on the satellite and the receiver on
32 the Earth [1–3]. The unit of TEC is defined as TECU which equals to 10^{16}
33 electrons/m² [3–7]. The slant path with respect to the local vertical at the position of
34 GPS receiver extends to the satellite as a function of elevation angle. The STEC (slant
35 TEC) calculated along the path of the GPS signal can be projected into the VTEC
36 (vertical TEC) by using mapping function [5,8]. VTEC values vary from several to
37 hundreds TECU due to solar cycle, geographical latitude and longitude, diurnal
38 variations, seasonal variations, geomagnetic effects and seismic activities [9,10].

39 Besides, global ionospheric models distributed by several organizations such as IGS
40 CODE (International GNSS Service, Centre for Orbit Determination in Europe), ESA
41 (European Space Agency), JPL (Jet Propulsion Laboratory), IRI (International
42 Reference Ionosphere) can also be alternative by interpolating TEC data nearest to the
43 corresponding position of the GPS receiver [5,11–14].

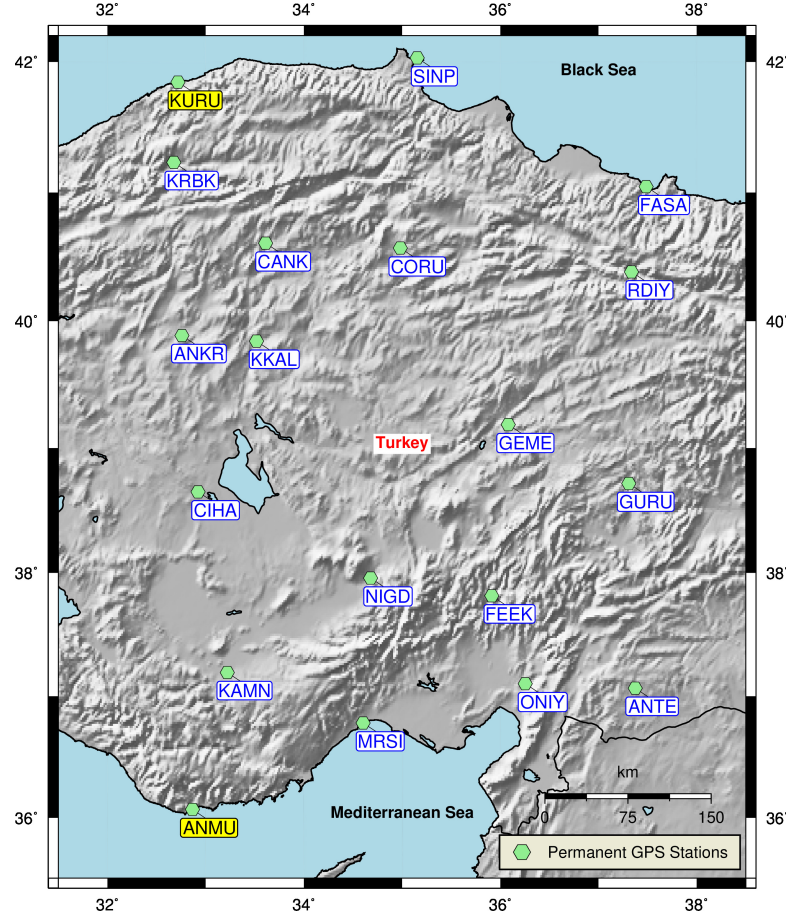
44 Since both the GPS receivers on the ground are sparse to model regional grid of TEC
45 and also global TEC models have limited accuracy, artificial neural networks are
46 preferred for predictive modeling of ionosphere [15–19]. Not only ionospheric
47 variations but also mean temperature predictions [20], solar radiation forecasting [21],
48 meteorological predictions [22] or tropospheric estimations [23] were recently studied
49 using neural network models to better interpret the geophysical processes over the
50 Earth. On the other hand, the spatial and time-dependent components of the
51 ionospheric activity need to be considered to predict VTEC variations in high spatial
52 and temporal accuracy [18, 24, 25]. Okoh et al. [18], Homam [24] and Mallika et al.
53 [25] investigated the neural network performances in terms of VTEC predictions
54 associated with the spatio-temporal contributors over Equatorial Region. Homam [24]
55 adopted a data acquisition methodology related to the occurrence of ionospheric
56 scintillation over a GPS station in Malaysia in order to integrate into neural network
57 modeling for VTEC predictions. Okoh et al. [18] argued about the effectiveness of the
58 foF2 storm model derived from IRI products, in which it was used as an additional
59 neuron for the neural input layer in their study over Nigeria. Mallika et al. [25]
60 investigated the performance of the neural networks in predicting VTEC variations
61 over India using dense global dataset of IRI models, but with limited ground-based
62 observations for neural network training and model testing. In this study, it is aimed
63 to predict significant GPS VTEC based on artificial neural network modeling using

64 dense ground-based observations obtained from permanent GPS stations within a
65 regional subnetwork over Central Anatolia in Turkey. The neural network model
66 proposed here depends on an approach, which contains network training by using a
67 bulk of GPS data acquired from 19 permanent stations for the period of 2015-2019
68 and validation of NN VTEC predictions in 2020 with respect to the GPS VTEC and
69 IRI2012 VTEC at the two northernmost and southernmost GPS stations, KURU and
70 ANMU, in the mid-latitude region.

71 **2. Materials and methods**

72 *2.1. GPS dataset and analysis*

73 GPS data processed within the scope of this study were obtained from the TUSAGA-
74 Aktif (Turkish National Permanent GPS Network-Active) and IGS networks over
75 Central Anatolia in Turkey (Figure 1). The RINEX (Receiver Independent Exchange
76 Format) files with 30 seconds measurement interval in the 24 hours of observation
77 span were downloaded from the IGS [26] and TUSAGA-Aktif [27] websites. The
78 GPS network consisting of 19 permanent stations covers an area from 36.2°E to
79 37.5°E in longitudes and 36.0°N to 42.0°N in latitudes. Supplementary Table S1
80 summarizes the detailed descriptions about the permanent GPS stations. The GPS
81 dataset was generated by selecting specific daily GPS observations in the range of
82 years for 2015-2020.



83

84 **Figure 1.** GPS network at the central region of Turkey used in this study.

85 In order to derive the total electron content at the locations of permanent stations,
 86 GPS data were processed using the GPS-TEC analysis (Ver. 3.0) software developed
 87 by Gopi Krishna Seemala [28]. The software calculates STEC along the slant
 88 trajectory. The STEC along the slant trajectory can be extracted from the geometry-
 89 free linear combination of GPS observations as per following Eq. (1) [29]:

$$90 \quad STEC = \frac{f_1^2 \cdot f_2^2}{40.3082 \frac{m^3}{s^2} \cdot (f_1^2 - f_2^2)} \{ (P_2 - P_1) - (b_P^s + b_P^r) \} \quad (1)$$

91 where; P_1 and P_2 are pseudorange observables corresponding to the high ($f_1=1575.42$
 92 MHz) and low ($f_2=1227.6$ MHz) GPS frequencies respectively, b_P^s is the pseudorange
 93 satellite delay and b_P^r is the pseudorange receiver delay. However, the STEC must be
 94 then converted to the VTEC considering a spherical thin-shell model for the
 95 ionosphere. According to the SLM (single layer model), a very thin layer at a fixed
 96 height above the Earth's surface contains all the free electrons [6].

97 Thus, as given in following equations, VTEC at ionospheric pierce point is derived

98 using a mapping function [7,30,31] based on the SLM:

99
$$STEC = VTEC \cdot M(z) + (b_s + b_r + b_{rx}) \quad (2)$$

100 with

101
$$M(z) = \frac{1}{\cos z^1} = \frac{1}{\sqrt{1 - \sin^2 z^1}} \quad (3)$$

102
$$\sin z^1 = \frac{R}{R+H} \cdot \sin z \quad (4)$$

103 where; $M(z)$ is the mapping function, R is the Earth's mean radius, b_s is satellite bias,
104 b_r is receiver bias, b_{rx} is receiver interchannel bias, H is the ionospheric layer height, z
105 and z' are the zenith angles at the receiver site and at the ionospheric pierce point,
106 respectively. In this study, the ionospheric layer was assumed at a fixed height of 350
107 km above the Earth's surface. In addition, the sampling rate of each GPS receiver was
108 30 seconds and the minimum elevation angle criterion was assumed to be 30° in case
109 any multipath effects might distort the GPS observations.

110 *2.2. Artificial Neural Network Approach*

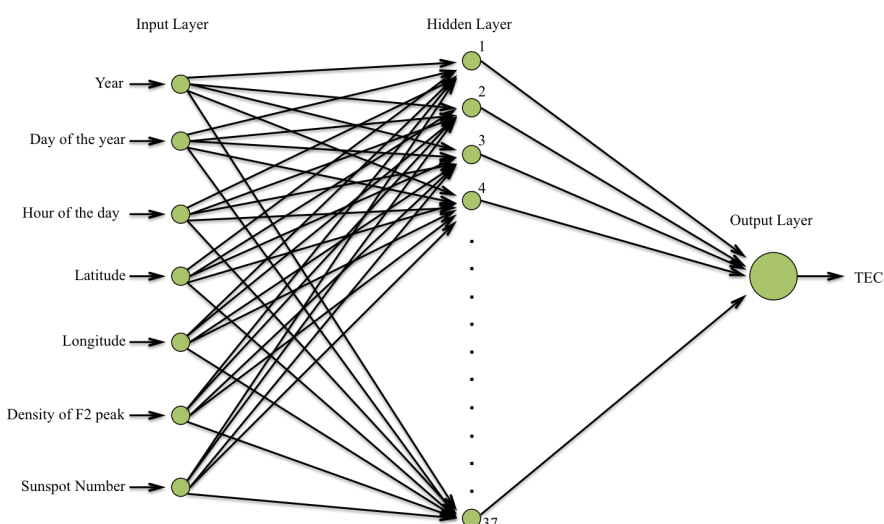
111 Neural networks are regarded as artificial intelligence mechanisms that can be trained
112 and are able to learn to deal with non-linear input/output relationships in the
113 complicated processes [32,33]. The mechanism contains simple processing elements
114 named as artificial neurons, in which the summation provided by manipulating the
115 input signal using weights is stored. The determination of the weights of the input
116 signal in an artificial neural network is realized by an iterative adjustment procedure
117 during the training process until the optimum weights are achieved [34]. Once the
118 neural network is trained, the input signal passes through an activation function
119 (transfer function) to generate output of neurons. Sigmoid activation function given in
120 Eq. (5) is usually preferred as activation function in multi-layer perceptron model.

121
$$f(x) = \frac{1}{1 + e^{-x}} \quad (5)$$

122 The activation function serves as non-linear filter to generate output signal. During
123 the training stage, a back-propagation algorithm is applied in feed-forward and feed-
124 backward processes. In an iterative approach, the biases of the neural network are
125 adjusted repeatedly until the RMSE (root mean square error) reaches a threshold
126 value for the output signal. In this study, the activation function of all layers is the

127 sigmoid function and Levenberg-Marquardt back-propagation algorithm was applied
128 to train the network.

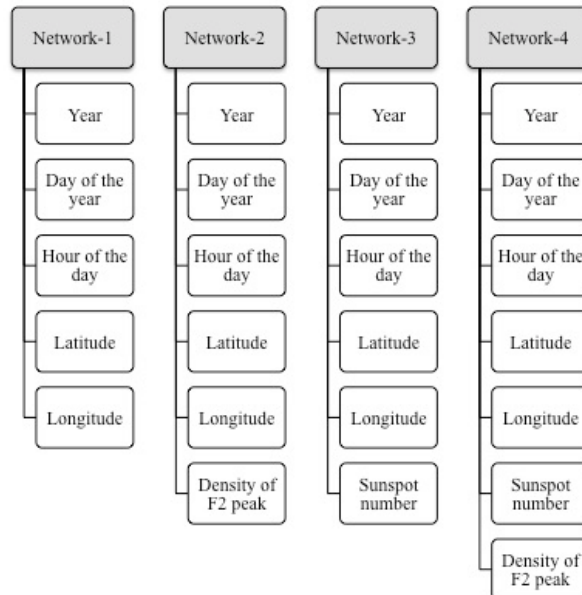
129 Due to its quick response for predictions and effectiveness during training process, the
130 multi-layer perceptron neural network consisting of one input layer, one hidden layer
131 with many neurons and one output layer was preferred in this study. The optimal
132 number of neurons and layers can be decided in consequence of trial and error as per
133 each specific problem [35]. The strategy followed here to determine the optimal
134 number of neurons in hidden layer was realized using different neural network
135 designs with varying input neurons. Since VTEC is associated with the solar cycle
136 variations, seasonal variations, diurnal variations, spatial variations and solar activity
137 variations, the proposed neural network herein was anticipated to learn considering
138 those parameters. The data about the sunspot numbers were provided from the
139 website of World Data Center Sunspot Index and Long-term Solar Observations [36].
140 Additionally, the relationship between VTEC and electron density at F2 peak ($NmF2$)
141 has a strong positive correlation [37,38] so that the learning stage of the network was
142 considered to be more effective by incorporation of the $NmF2$ data obtained from the
143 IRI model [39]. Furthermore, the IRI is an empirical ionospheric model that
144 introduces reliable global data accompanying with long-term solar cycle variations
145 [18]. Accordingly, the input layer of our neural network contains seven neurons
146 namely year, day of the year, hour of the day, latitude, longitude, sunspot number and
147 electron density at F2 peak (Figure 2).



148

149 **Figure 2.** The structure of the multi-layer perceptron neural network with one
150 hidden layer used in this research.

151 Using the different combinations of input neurons, several network designs were
152 statistically tested for the determination of the optimal architecture of the neural
153 network. The different neural networks were designed from the simplest structure to
154 more complex one, in which varying parameters and numbers of input neurons were
155 considered (Figure 3).



156

157 **Figure 3.** The different neural network designs with the corresponding input
158 neurons in each.

159 Considering a test procedure to determine which network design was the most
160 appropriate for network training, each of four network designs was simulated 50 times
161 in terms of varying numbers of neurons in the hidden layer. The decision criterion of
162 the testing procedure was the RMSE parameter statistically expected to be the lowest
163 based on the predictions in the neural networks [40].

164 The analyses within this research covers the period between 2015 and 2020. The
165 strategy to constitute a dataset was adopted by selecting the days with the weakest
166 ionospheric activity for each month. Hourly-averaged VTEC values calculated from
167 GPS observations were the output signal of the neural network. It is worth to say that
168 the training dataset differs from the dataset used in the random model testing. In the
169 random testing, the proposed model has been assessed in terms of the temporal
170 performance. The dataset for the period of 2015-2019 was acquired from all the
171 permanent stations performing in the GPS network demonstrated in Suppl. Figure 1
172 and allocated to training by 70% of it, validation by 15% of it and testing by 15% as

of remaining. This training dataset was randomly selected among the daily GPS data acquired in those permanent GPS stations during the weakest day of each month in a year, which means that each station provides data of 4 out of 12 random weakest days in a year. Apart from this dataset used to train the neural network, the GPS data for the year of 2020 acquired from KURU (41.846°N , 32.718°E) and ANMU (36.069°N , 32.865°E) permanent stations were randomly used to test the neural network model. There were two criteria for the data selection in random testing stage, as one of them was to use the data out of the training dataset period, which were 2020 GPS data here and the other was choosing the northernmost and the southernmost stations to notice the spatial variations. In addition, the diurnal performance of the neural network was tested for different times of a day namely 03:00 UTC (Coordinated Universal Time) equivalent to 06:00 Local Time, 09:00 UTC (12:00 Local Time), 15:00 UTC (18:00 Local Time) and 21:00 UTC (00:00 Local Time), which correspond to near the time of sunrise, the noontime with high ionospheric level, near the time of sunset and the midnight, respectively. Besides, in order to test the seasonal performance of the neural network, the predictions were also tested for different seasons in 2020 namely vernal equinox, summer solstice, autumnal equinox and winter solstice.

The performance of our neural network was assessed in terms of the absolute and relative errors estimated using following equations, respectively:

$$|E_{abs}| = |TEC_{NN} - TEC_{GPS}| \quad (6)$$

$$|E_{rel}| = \left(\frac{|E_{abs}|}{TEC_{GPS}} \right) \times 100 \quad (7)$$

where; E_{abs} is the absolute error, E_{rel} is the relative error, TEC_{NN} and TEC_{GPS} are predicted VTEC by the neural network and GPS-derived VTEC, respectively [19,41]. In this context, the less the absolute and relative errors, the closer the predicted VTEC values by neural network model and calculated VTEC values from GPS observations.

3. Results and discussions

First, in order to determine the optimum architecture of the neural network, all the proposed neural network designs were compared based on the RMSEs for the dataset period between 2015 and 2019. In this research, the RMSEs indicating the deviations of predicted VTEC by the neural network (hereinafter referred to as NN VTEC) from

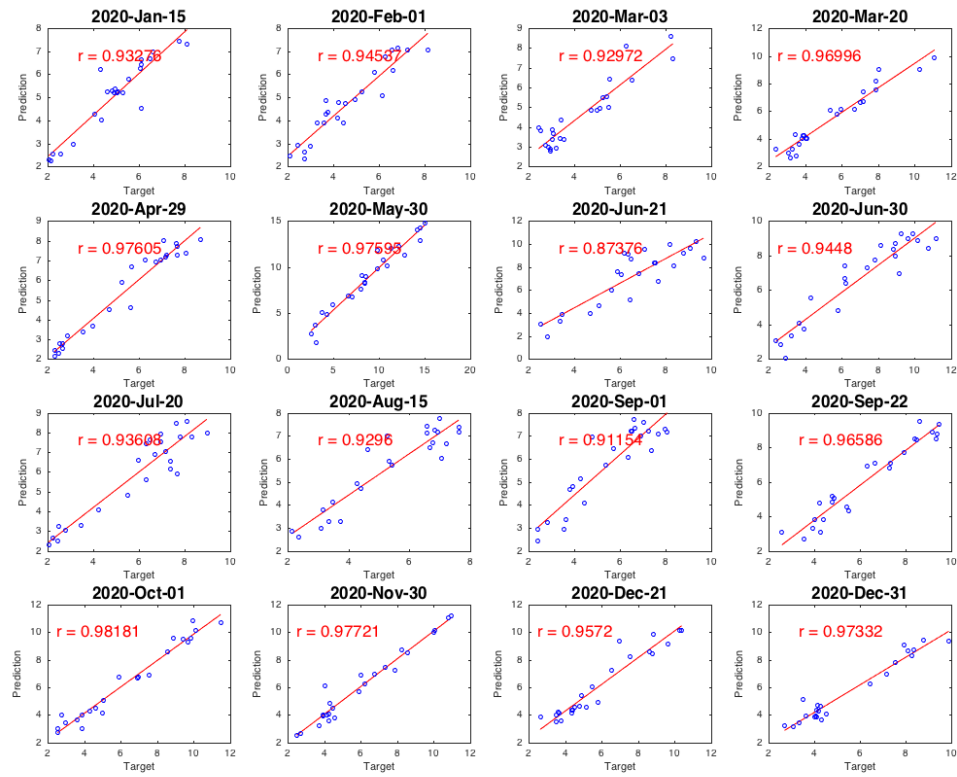
203 observed VTEC by means of GPS (hereinafter referred to as GPS VTEC) were
204 calculated per the number of neurons in hidden layer for each network designs
205 individually. Both in Suppl. Figure S1 and Figure S2, it is evidently proven that the
206 Net4 consisting of seven input neurons namely the year, day of the year, hour of the
207 day, latitude, longitude, sunspot number, density of F2 peak neurons has the lowest
208 RMSE compared to other three network designs. The RMSE for the dataset of KURU
209 and ANMU stations has the minimum value (~1.2 TECU) for the simulation test
210 using 37 neurons in the hidden layer, which indicates the best agreement between the
211 NN VTEC and GPS VTEC (Suppl. Figure S2). Thus, the training of the network was
212 achieved using seven neurons in the input layer and 37 neurons in the hidden layer.

213 Besides, it is clear that the higher the RMSE, the worst the neural network design
214 performance. The first neural network design (Net1) has the highest RMSEs
215 compared to other network designs that means the fewer input neurons in, the poorer
216 the network performance. Furthermore, the second (Net2) and third (Net3) neural
217 network designs have moderate performances compared to the Net1 (the worst) and
218 the Net4 (the best). As a result, the increase in the number of input neurons helps the
219 neural network to learn better and to make more reasonable predictions.

220 In Figure 4 and Figure 5, the NN VTEC (prediction in the vertical axis) versus the
221 GPS VTEC (target in the horizontal axis) was plotted for KURU and ANMU stations
222 for the 2020 dataset, respectively. The scatter plots for the predictions and their
223 corresponding targets demonstrate the red lines of best fitting for regression model
224 together with the correlation coefficients (r). It is a fact that there is a high correlation
225 between NN VTEC and GPS VTEC since all the correlation coefficients except the
226 lowest two are above 0.9 for both KURU and ANMU stations. The lowest correlation
227 coefficients were 0.87376 for KURU station in June 21, 2020 and 0.84408 for ANMU
228 station in July 20, 2020.

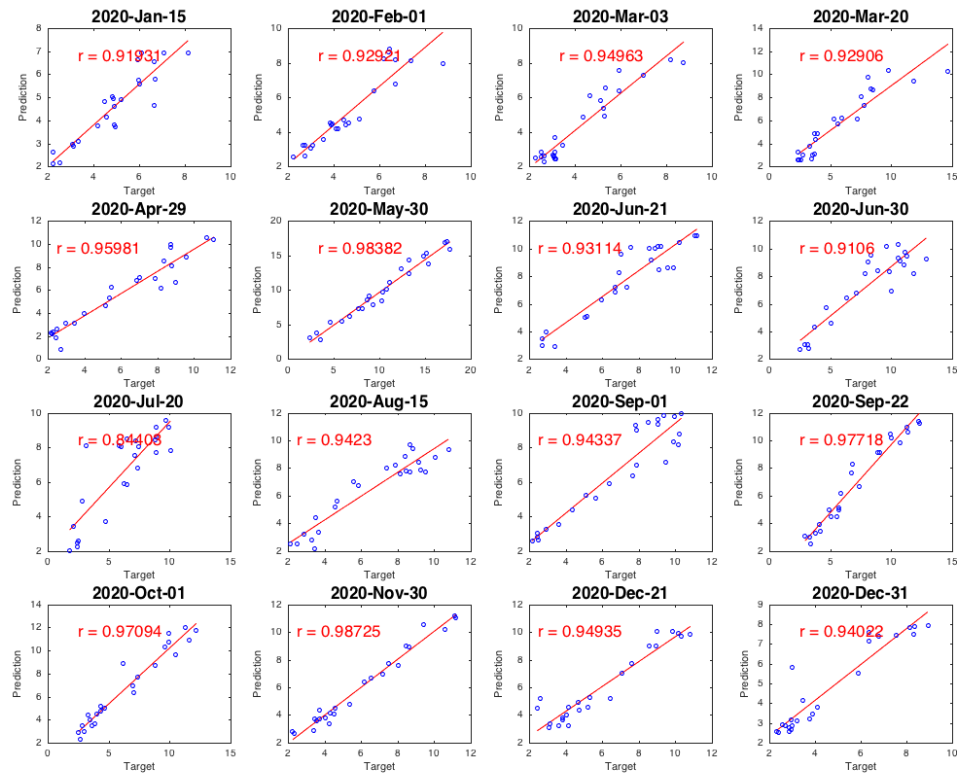
229

230 **Figure 4.** The correlations between the NN VTEC and the GPS VTEC for the 2020
 231 dataset over KURU station.



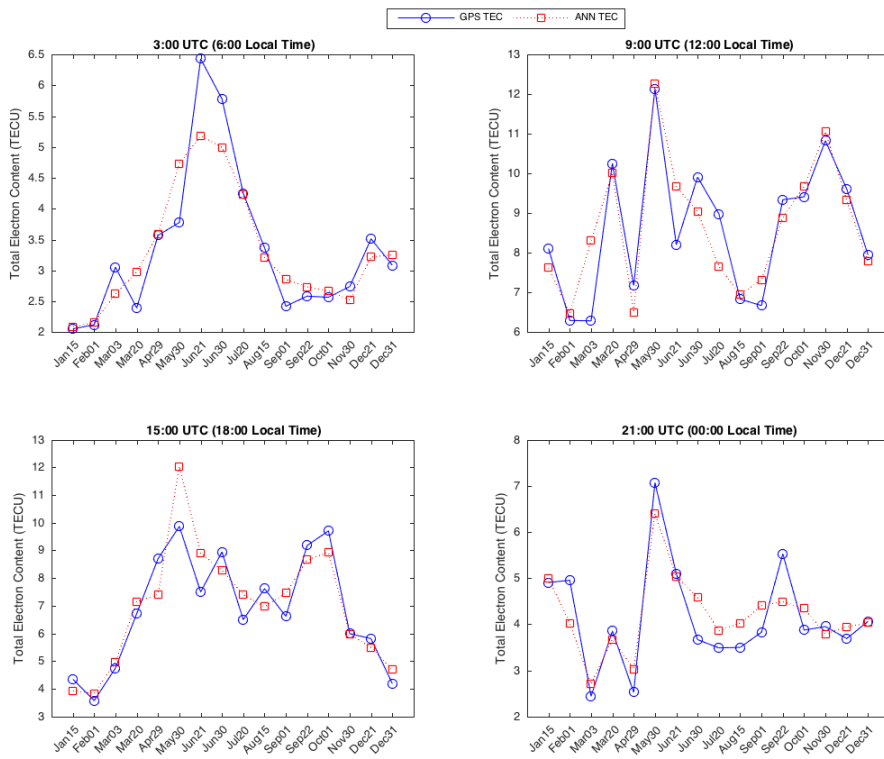
232

233 **Figure 5.** The correlations between the NN VTEC and the GPS VTEC for the 2020
 234 dataset over ANMU station.



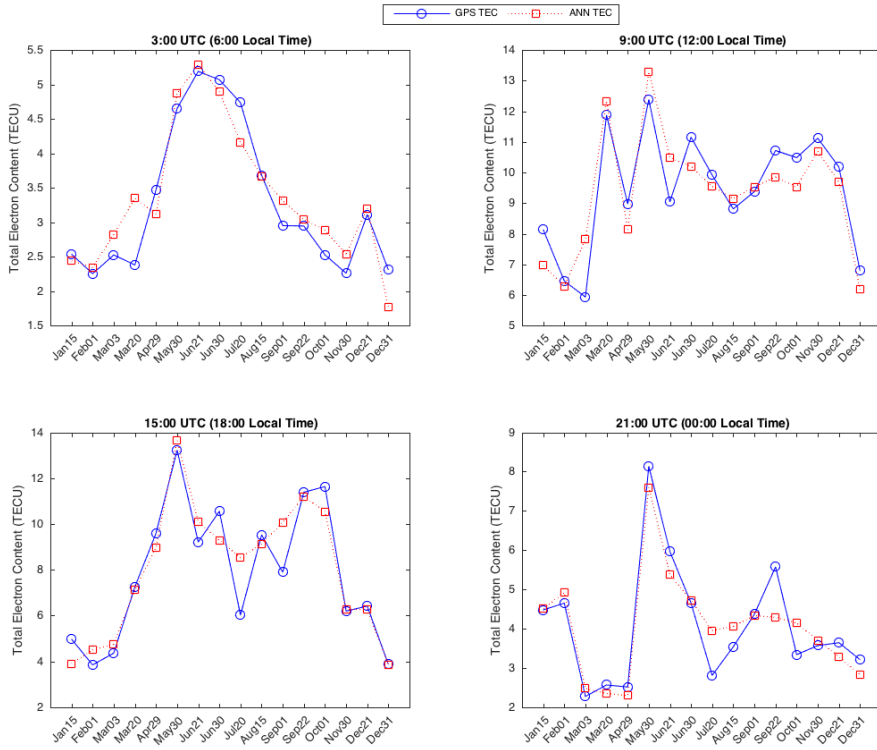
235 In order to evaluate the diurnal performance of the neural network, NN VTEC was
 236 compared with the corresponding GPS VTEC for the specific times of the day during
 237 2020 over KURU and ANMU stations. These times within the day were determined
 238 based on the positions of the sun with respect to the local during the day as the near
 239 the time of sunrise, the noontime with high ionospheric level, near the time of sunset
 240 and the midnight. Thus, 03:00 UTC (06:00 Local Time), 09:00 UTC (12:00 Local
 241 Time), 15:00 UTC (18:00 Local Time) and 21:00 UTC (00:00 Local Time) were
 242 considered as the benchmarks for intraday variations. The local time in Turkey is 3
 243 hours ahead of the universal time.

244 The NN VTEC obtained from the neural network model and GPS VTEC calculated
 245 from the GPS observations were compared in hourly basis for those specific times of
 246 the day during 2020 over KURU and ANMU stations (Figure 6 and Figure 7).
 247 Additionally, the absolute and relative errors of NN VTEC from GPS VTEC for those
 248 specific times of the day during 2020 over KURU and ANMU stations were
 249 demonstrated, respectively, in Supplementary Figure S3-S6. From those figures, it is
 250 evident that the predictions (NN VTEC) for the specific times of the day during 2020
 251 are highly correlated with the targets (GPS VTEC) since the highest absolute errors
 252 does not exceed the value of 2.5 TECU during 2020 over both stations.



253

254 **Figure 6.** Hourly comparison of NN VTEC and GPS VTEC over KURU station.



255

256 **Figure 7.** Hourly comparison of NN VTEC and GPS VTEC over ANMU station.

257

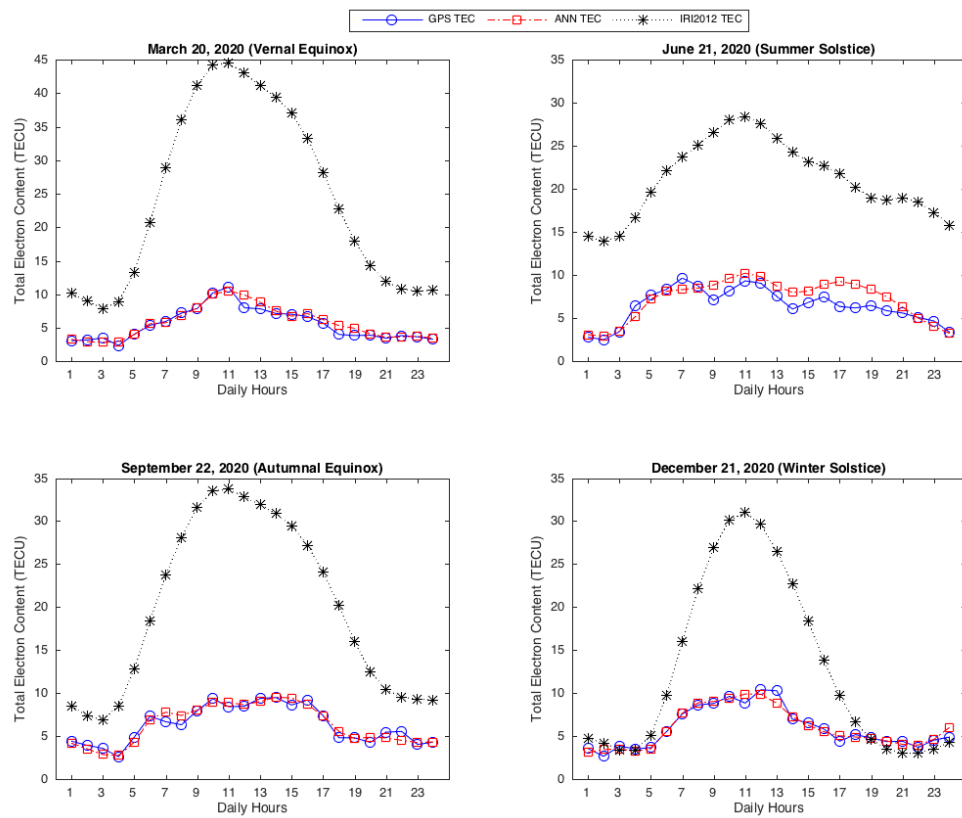
Table 1. The correlation coefficients for the comparison of the specific day times

Station	03:00 UTC	09:00 UTC	15:00 UTC	21:00 UTC
KURU	0.91149	0.87642	0.85907	0.91008
ANMU	0.93391	0.89154	0.93463	0.92716

258 As seen from the plots in Figure 6 and Figure 7, the NN VTEC and GPS VTEC at all
 259 day times over both KURU and ANMU stations have mostly similar trends during
 260 2020 indicating good predictions for the GPS VTEC. The NN VTEC and GPS VTEC
 261 indicate the goodness of fitting with the correlation coefficient of more than 0.85 for
 262 different day times over KURU and ANMU stations (Table 1). In Supplementary
 263 Figure S3 and Figure S4, it is noticed that the absolute errors over those stations are
 264 less than 2.5 TECU throughout the year. Accordingly, the maximum relative errors
 265 are less than the limits of 35% and 45% over KURU and ANMU stations,
 266 respectively (Suppl. Figure S5 and Figure S6).

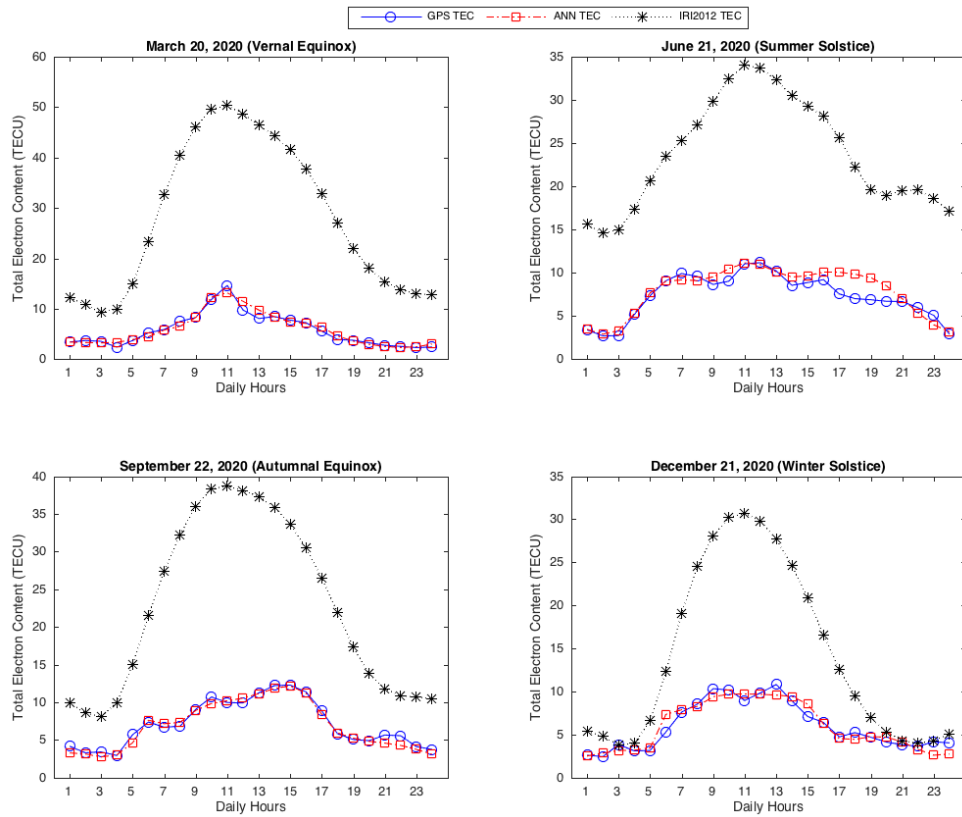
267 On the other hand, another perspective in evaluating the performance of the neural
 268 network is based on the seasonal variations of VTEC. Thus, the different seasons in
 269 2020 namely vernal equinox, summer solstice, autumnal equinox and winter solstice
 270 were considered to investigate the seasonal variations. In the seasonal evaluation

process, the IRI2012 VTEC derived from IRI2012 model using NeQuick parameter for the Ne topside was also incorporated into the analysis in order to compare the neural network model with an international reference model. Accordingly, the seasonal comparison of the NN VTEC with the GPS VTEC and the IRI2012 VTEC was demonstrated in Figure 8 and Figure 9. As also seen from the correlation coefficients, it is very clear that the NN VTEC provides much better correlation with the GPS VTEC than the IRI2012 VTEC has (Table 2).



278

279 **Figure 8.** The seasonal comparison of the NN VTEC and the IRI2012 VTEC with
280 the GPS VTEC during 2020 over KURU station.



281

282 **Figure 9.** The seasonal comparison of the NN VTEC and the IRI2012 VTEC with
283 the GPS VTEC during 2020 over ANMU station.

284

Table 2. The correlation coefficients for the comparison of seasonal variations.

Station Code	Model	Vernal Equinox (March 20)	Summer Solstice (June 21)	Autumnal Equinox (September 22)	Winter Solstice (December 21)
KURU	NN VTEC	0.95349	0.92844	0.96560	0.96070
	IRI2012 VTEC	0.94893	0.85616	0.91466	0.94949
ANMU	NN VTEC	0.97437	0.92746	0.98680	0.95510
	IRI2012 VTEC	0.91737	0.90834	0.91173	0.96866

285

4. Conclusions

286 The GPS data obtained from the TUSAGA-Aktif and IGS networks over the Central
287 Anatolia in Turkey was used as the output of this research. The GPS network
288 consisting of 19 permanent stations provided also random data for the training of the
289 neural network. The neural network structure was established using the seven input

neurons namely year, day of the year, hour of the day, latitude, longitude, sunspot number and electron density at F2 peak. The optimal numbers of the input neurons and the neurons in the hidden layer were determined as per the simulation tests aimed to reach the lowest RMSE. The neural network design with seven input neurons (Net4) verified the lowest RMSE compared to the other network designs. The simulation tests demonstrated that the more input neurons integrated into the input layer, the better the network training and the more significant the predictions. Additionally, the target GPS dataset for the neural network model has here played pivotal role. Unlike the targets used in the network training, it was aimed to achieve a network validation process using unique independent targets in the model testing. Thus, the target dataset was divided into two categories. The one for network training contains random GPS data acquired from 19 permanent stations during the period of 2015-2019. On the contrary, the model testing was accomplished by using a different bulk of targets calculated from the GPS observations in 2020. From this perspective, some significant indicators prove the applicability of the proposed model such that the correlations between the predictions for the NN VTEC and their corresponding targets for GPS VTEC have pointed out quite well fitting at the selected days in 2020. Those selected days were determined as per the weakest ionospheric activity within each month during the year. Using this multi-layer perceptron model, the diurnal variations of VTEC can be predicted quite well by the proposed neural network structure at the specific day times since the absolute and relative errors in TECU are very low. The correlation coefficients also simply demonstrate well fitting for diurnal predictions, indicating that the different day times are not deterrent in the modeling. Considering the correlation coefficients and the absolute errors of the NN VTEC from the GPS VTEC, the seasonal comparison of the NN VTEC with the GPS VTEC notices the high accurate prediction capability of the neural network model during different seasons in 2020. During equinox seasons, the ANMU station evidently demonstrates better in fitting with the proposed neural network while the KURU station outperforms during summer and winter solstices. As also expected, during the all seasons in 2020, the NN VTEC provides better predictions for the seasonal variations than the IRI2012 VTEC obtained from the global IRI model. To conclude, instead of competing with the global models like IRI, the proposed model in this study is there to elaborate the power of such neural network models in predicting the VTEC since those models could be a well contributor to improve the regional models.

324 **Declaration of Competing Interest**

325 The author declares that he has no known competing financial interests or personal
326 relationships that could have appeared to influence the work reported in this paper.

327 **References**

- 328 [1] Y. Huang, K. Cheng, S. Chen, On the equatorial anomaly of the ionospheric
329 total electron content near the northern anomaly crest region, *Journal of*
330 *Geophysical Research: Space Physics*. 94 (1989) 13515–13525.
- 331 [2] R.G. Rastogi, J.A. Klobuchar, Ionospheric electron content within the
332 equatorial F 2 layer anomaly belt, *Journal of Geophysical Research: Space*
333 *Physics*. 95 (1990) 19045–19052.
- 334 [3] B. Hofmann-Wellenhof, H. Lichtenegger, J. Collins, Global positioning
335 system: theory and practice, Springer Science & Business Media, 2012.
- 336 [4] G. Seeber, Satellite Geodesy: Foundations, Methods and Applications,
337 *International Hydrographic Review*. 4 (2003) 92–93.
- 338 [5] S. Schaer, Mapping and predicting the Earth's ionosphere using the Global
339 Positioning System, Ph.D. Thesis, Astronomical Institute, University of Bern.
340 (1999).
- 341 [6] U. Wild, Ionosphere and geodetic satellite systems: permanent GPS tracking
342 data for modelling and monitoring., *Geod.-Geophys. Arb. Schweiz.* 48 (1994).
- 343 [7] A.J. Mannucci, B.D. Wilson, C.D. Edwards, A New Method for Monitoring
344 the Earth's Ionospheric Total Electron Content Using the GPS Global Network,
345 in: Proceedings of the 6th International Technical Meeting of the Satellite
346 Division of The Institute of Navigation (ION GPS 1993), 1993: pp. 1323–
347 1332.
- 348 [8] J.S. Shim, Analysis of total electron content (TEC) variations in the low-and
349 middle-latitude ionosphere, Ph.D. Thesis. (2009).
- 350 [9] R. Warnant, E. Pottiaux, The increase of the ionospheric activity as measured
351 by GPS, *Earth, Planets and Space*. 52 (2000) 1055–1060.

- 352 [10] G. Liu, W. Huang, J. Gong, H. Shen, Seasonal variability of GPS-VTEC and
353 model during low solar activity period (2006-2007) near the equatorial
354 ionization anomaly crest location in Chinese zone, *Advances in Space*
355 *Research.* 51 (2013) 366–376. <https://doi.org/10.1016/j.asr.2012.09.002>.
- 356 [11] D. Bilitza, D. Altadill, Y. Zhang, C. Mertens, V. Truhlik, P. Richards, L.-A.
357 McKinnell, B. Reinisch, The International Reference Ionosphere 2012—a model
358 of international collaboration, *Journal of Space Weather and Space Climate.* 4
359 (2014) A07.
- 360 [12] S.K. Leong, T.A. Musa, K. Omar, M.D. Subari, N.B. Pathy, M.F. Asillam,
361 Assessment of ionosphere models at Banting: Performance of IRI-2007, IRI-
362 2012 and NeQuick 2 models during the ascending phase of Solar Cycle 24,
363 *Advances in Space Research.* 55 (2015) 1928–1940.
- 364 [13] R. Scharroo, W.H.F. Smith, A global positioning system-based climatology for
365 the total electron content in the ionosphere, *Journal of Geophysical Research:*
366 *Space Physics.* 115 (2010) A10318.
- 367 [14] W. Wan, F. Ding, Z. Ren, M. Zhang, L. Liu, B. Ning, Modeling the global
368 ionospheric total electron content with empirical orthogonal function analysis,
369 *Science China Technological Sciences.* 55 (2012) 1161–1168.
- 370 [15] A.J. Coster, J.C. Foster, P.J. Erickson, Monitoring the ionosphere with GPS,
371 *GPS World.* 14 (2003).
- 372 [16] Z. Liu, Y. Gao, Ionospheric TEC predictions over a local area GPS reference
373 network, *GPS Solutions.* 8 (2004) 23–29.
- 374 [17] A. Vernon, L.R. Cander, Regional GPS receiver networks for monitoring local
375 mid-latitude total electron content, *Annals of Geophysics.* 45 (2002) 649–656.
- 376 [18] D. Okoh, O. Owolabi, C. Ekechukwu, O. Polarim, G. Arhiwo, J. Agbo, S.
377 Bolaji, B. Rabiu, A regional GNSS-VTEC model over Nigeria using neural
378 networks: A novel approach, *Geodesy and Geodynamics.* 7 (2016) 19–31.
- 379 [19] R.F. Leandro, M.C. Santos, A neural network approach for regional vertical

- 380 total electron content modelling, *Studia Geophysica et Geodaetica*. 51 (2007)
381 279–292. <https://doi.org/10.1007/s11200-007-0015-6>.
- 382 [20] M. Ding, A neural network model for predicting weighted mean temperature,
383 *Journal of Geodesy*. 92 (2018) 1187–1198.
- 384 [21] S. Pereira, P. Canhoto, R. Salgado, M.J. Costa, Development of an ANN based
385 corrective algorithm of the operational ECMWF global horizontal irradiation
386 forecasts, *Solar Energy*. 185 (2019) 387–405.
- 387 [22] A. Manzato, A. Pucillo, A. Cicogna, Improving ECMWF-based 6-hours
388 maximum rain using instability indices and neural networks, *Atmospheric*
389 *Research*. 217 (2019) 184–197.
- 390 [23] M.O. Selbesoglu, Prediction of tropospheric wet delay by an artificial neural
391 network model based on meteorological and GNSS data, *Engineering Science*
392 and Technology, an International Journal. 23 (2020) 967–972.
- 393 [24] M.J. Homam, Prediction of total electron content of the ionosphere using
394 neural network, *Jurnal Teknologi*. 78 (2016).
- 395 [25] L. Mallika I, D.V. Ratnam, S. Raman, G. Sivavaraprasad, Performance analysis
396 of Neural Networks with IRI-2016 and IRI-2012 models over Indian low-
397 latitude GPS stations, *Astrophysics and Space Science*. 365 (2020) 1–14.
- 398 [26] URL-1, International GNSS Service, (n.d.). <https://igs.org/> (accessed January
399 31, 2022).
- 400 [27] URL-2, TUSAGA-Aktif, (n.d.). <https://www.tusaga-aktif.gov.tr/> (accessed
401 January 31, 2022).
- 402 [28] URL-3, GPS-TEC analysis software, (n.d.). <http://seemala.blogspot.com>
403 (accessed January 31, 2022).
- 404 [29] M.A. Sharifi, S. Farzaneh, Local Ionospheric Modeling Using the Localized
405 Global Ionospheric Map and Terrestrial GPS, *Acta Geophysica*. 64 (2016)
406 237–252.

- 407 [30] Y. Norsuzila, M. Abdullah, M. Ismail, Leveling Process of Total Electron
408 Content(TEC) Using Malaysian Global Positioning System(GPS) Data,
409 American Journal of Engineering and Applied Sciences. 1 (2008).
- 410 [31] Y. Xiang, Y. Gao, An enhanced mapping function with ionospheric varying
411 height, Remote Sensing. 11 (2019) 1497.
- 412 [32] L.R. Cander, M.M. Milosavljevic, S.S. Stankovic, S. Tomasevic, Ionospheric
413 forecasting technique by artificial neural network, Electronics Letters. 34
414 (1998) 1573–1574.
- 415 [33] R.F. Leandro, M.C. Santos, Comparison between autoregressive model and
416 neural network for forecasting space environment parameters, Bollettino Di
417 Geodesia e Scienze Affini. 63 (2004) 197–212.
- 418 [34] T. Kohonen, Adaptive, associative, and self-organizing functions in neural
419 computing, Applied Optics. 26 (1987) 4910–4918.
- 420 [35] P.K. Simpson, Artificial Neural Systems: Foundations Paradigms, Pergamon
421 Press, New York, 1990.
- 422 [36] URL-5, World Data Center SILSO, (n.d.). <https://wwwbis.sidc.be/silso/>
423 (accessed January 31, 2022).
- 424 [37] H. Jin, T. Maruyama, 3-3-2 Different behaviors of TEC and NmF2 observed
425 during large geomagnetic storms, Journal of the National Institute of
426 Information and Communications Technology Vol. 56 (2009).
- 427 [38] R. Leitinger, L. Ciraolo, L. Kersley, S.S. Kouris, P. Spalla, Relations between
428 electron contentand peak density: regular and extreme behaviour, Annals of
429 Geophysics. 47 (2004).
- 430 [39] URL-4, Community Coordinated Modeling Center (CCMC), (n.d.).
431 <https://ccmc.gsfc.nasa.gov> (accessed January 31, 2022).
- 432 [40] A.J. Conway, K.P. Macpherson, G. Blacklaw, J.C. Brown, A neural network
433 prediction of solar cycle 23, Journal of Geophysical Research: Space Physics.
434 103 (1998) 29733–29742.

435 [41] M.R.G. Razin, B. Voosoghi, A. Mohammadzadeh, Efficiency of artificial
436 neural networks in map of total electron content over Iran, *Acta Geodaetica et*
437 *Geophysica.* 51 (2016) 541–555. <https://doi.org/10.1007/s40328-015-0143-3>.

438 **Supplementary Material Link:**

439 https://github.com/aliozk4n/Supplementary_Material.git